LAWRENCE
LIVERMORE
NATIONAL
LABORATORY

UCRL-JRNL-207265

Synthesis and Thermal Stability of Amorphous Be-B-X Alloy Coatings

A. F. Jankowski, M. A. Wall, T. G. Nieh

October 15, 2004

Journal of NonCrystalline Solids

Synthesis and Thermal Stability of Amorphous Be-B-X Alloy Coatings

A.F. Jankowski, M.A. Wall, and T.G. Nieh

University of California, Lawrence Livermore National Laboratory, Livermore, CA 94550

ABSTRACT

Amorphous Be-B-X alloys are vapor deposited as coatings. The microstructure and hardness of the Be-B-X coatings are examined using transmission electron microscopy and nanoindentation, respectively. Whereas a Be-B-2.5 at.% Cu amorphous coating is found to crystallize to a cubic Be-33 at.% B phase at 673 K, a coating of Be-B-1.8 at.% Fe-0.4 at.% Cr-0.3 at.% Co does not crystallize until at a higher temperature of 748 K. The hardness of the amorphous Be-B-X coating increases with B content but is less than its crystalline counterparts.

PACS codes**: 61.14.Lj; 61.43.Dq; 61.46+w;61.66.Dk; 64.70.Kb; 68.37.Lp; 68.55.Nq; 68.60.Dv**

Key Words**: beryllium boride; sputter deposition; nanocrystalline; amorphous; metallic glass**

INTRODUCTION

Beryllium (Be) is a metal of major importance in the space and nuclear industries. [1-4] It has a low density, high elastic modulus, a high melting point of 1562 K, high heat capacity, and good nuclear hardness. For example, Be is ideal for space mirror sensors because of its low density and high micro-yield strength (i.e., the stress that gives rise to a plastic strain of 10^{-6}). [5] A high micro-yield strength is a requirement for components to remain undistorted during fast space maneuvers. However, Be suffers from some intrinsic problems such as low ductility, poor manufacturability, and toxicity, all of which limit its broad application. It's generally accepted that the low ductility is associated with its hexagonal close packed (hcp) structure, propensity for localized slip, and high impurity content (especially BeO). Previous efforts have been made to improve the ductility either by alloying to change the crystal structure from hcp to body centered cubic (bcc) or by forming intermetallic beryllides. [6-7] However, these approaches have met with little success. Although some binary and ternary phase diagrams were developed as a result of these efforts, general information on the phase relationships between Be and other elements is quite limited.

Hollow spheres of Be or with metals as Boron (B) that have a similar density to atomic number ratio, and with uniform wall thickness are sought for use as ablative fuel containers in plasma physics studies of inertial confinement fusion (ICF). [8] In addition, selective doping with a heavier element such as copper (Cu) at 1-2 at.% is useful to appropriately adjust the x-ray opacity of the Be shell, i.e. the ignition capsule. There are additional requirements for Be as ignition targets. The shells must be near atomically smooth, dense, isotropic, strong, and homogeneous. Elemental Be and Be-Cu shells can be formed as coatings using sputter deposition. [9-12] However, the anisotropic crystalline structure and the surface roughness that

scales with the columnar size of the deposits have been difficult to reduce to levels below 40 nm, even by ion irradiation. [12] An alternative path to achieve the desired properties for the Be coating is found in the characteristics typically attributed to nanocrystalline or amorphous alloys.

A eutectic at 11 at.% B is seen in the binary Be-B phase diagram. [13] Although it would appear that the Be-B eutectic may not be deep enough to be a potential glass former by melt spinning [14-15], the development of nanocrystalline and amorphous Be microstructures has been successfully demonstrated using vapor deposition for the Be-B alloy system. [11, 16] The rapid quench that is needed to stabilize a glassy solid phase can, in general, be accomplished from the gas phase by sputter deposition process. [17] The general effect of B and iron (Fe) impurity additions to vapor deposited Be is to refine the columnar structure and to dilate the host hexagonal close-packed (hcp) Be lattice. [11, 16] At B concentrations above the eutectic, fully amorphous Be-B coatings were produced. These coatings are relatively hard but are found to crystallize at anneal temperatures as low as 500 K. [18] Therefore, it is desirable to reduce the B content to avoid embrittlement and stabilize the amorphous structure by increasing its crystallization temperature. These objectives form the basis for the current development of Be-B-X alloys. In this study, the concentration of X is kept at an equivalent of 2.5 at.% (or less) in accordance with general design guidelines for Be-based ignition capsules. In particular, we examine the ternary (X = Cu) and pseudo-ternary (X = Fe-Cr-Co) alloys. For the later case, several metals of dissimilar crystalline systems are added with the intent of further delaying the onset of crystallization by frustrating the path to nucleation. [19-21]

EXPERIMENTAL PROCEDURES

The Be-B-X coatings are sputter deposited onto polished Si(111) wafers at a 6 cm separation distance above an array of three 3.3 cm diameter planar magnetrons equally spaced along the circumference of a 7 cm diameter circle. Each target material is rate calibrated for collective use to create a desired coating composition. The 0.999 pure B, >0.994 pure Be, and $Be_{.94}Cu_{.06}$ targets were fabricated by the hot-isostatic pressing of powder metal precursors in sealed, evacuated tantalum containers. These three targets are co-sputtered to produce the Be-B-Cu coatings. For the Be-B-X coatings where X = $Fe_{.71}Cr_{.16}Co_{.13}$, a case carburizable stainless steel alloy (CSS-42L^{TM}) of base composition $Fe_{.668}Cr_{.152}Co_{.120}Mo_{.028}Ni_{.019}V_{.007}C_{.006}$ is sputtered along with the Be and B targets. (For the low concentrations of stainless steel used in this study, the presence of dopant elements other than Fe, Cr, and Co was immeasurable from x-ray spectra.) The deposition chamber is cryogenically pumped to a 5×10^{-6} Pa base pressure. A 0.25-0.4 Pa sputter gas pressure of Ar is maintained using a using a 25-35 cm^3-min^{-1} total flow rate. Calibrated deposition rates of the B, Be, $Be_{0.94}Cu_{0.06}$, and steel targets (with respect to forward target power) are 0.066, 0.165, 0.374, and 0.108 nm-$(W\text{-}min)^{-1}$, respectively. The composition of target and representative coatings are confirmed through thickness measurements using contact profilometry, and by electron microprobe measurements as referenced to calibration standards.

The 0.2-3 μm thick coatings are prepared in cross-section for transmission electron microscope (TEM) imaging and diffraction analysis. In the preparation of samples for cross-section, two wafer pieces are epoxied face-to-face and then encapsulated in a metal tube from which 0.2-0.4 mm thick disks are cut. [22] The 3 mm diameters disks are then lapped to less than 0.1 mm, dimpled, and ion milled. Bright field or high resolution imaging is used to reveal the

presence or lack of a microstructure, and selected-area diffraction (SAD) patterns are used to determine crystalline phases when present. To assess the stability of the as-deposited structure, the samples are vacuum annealed in-situ during TEM imaging. The temperature of the specimen holder is initially heated to 473 K and then increased to 773 K in 25 K increments with a 5-7.5 min. hold time at each temperature. Above 773 K, the integrity of the cross-sectioned sample becomes compromised. The accuracy of measuring the sample temperature has been calibrated to ±10 ºC based on known phase transformations.

The coating hardness is measured using a Nanoindenter^{TM}. A Berkovitz diamond tip that has three-sides, each at 65.3˚ to the base, is used to indent the surface of the coatings. Force measurements are repeated and averaged at various depths. Standard deviations are used to derive the probable errors. Hardness is defined as the average pressure under the indenter tip that can be calculated from the load divided by the projected area of contact between the tip and the sample. The projected area is determined from the depth of penetration using the known profile of the tip. Hardness is computed using a standard analysis procedure although there are limitations imposed by analyzing inhomogeneous and hard materials. [23] Values are reported at a penetration depth no more than one-third of the coating thickness.

RESULTS

The $Be_{1-m-n}B_nX_m$ coatings fabricated for electron microscopy examination are comprised of X = Cu (m = .025 with n = .151) and X = $Fe_{.71}Cr_{.16}Co_{.13}$ (m = .009 with .133< n <.305; and m = .025 with .056< n <.337). The $Be_{.823}B_{.151}Cu_{.025}$ sample is amorphous in the as-deposited condition as seen in the high resolution image and SAD pattern (of Fig. 1a). The positions of

individual Si atoms, at the bottom of Fig. 1a, are resolved perpendicular to the (111) wafer orientation. The $Be_{.823}B_{.151}Cu_{.025}$ coating starts on the amorphous native-oxide layer of silica. Up to 673 K, the sample remains amorphous and then appeared to spontaneously transform into the crystallized microstructure seen in Fig. 1b – an equiaxed crystal structure as confirmed in the SAD pattern insert. The interplanar spacings that correspond to the SAD (of Fig. 1b) are listed in Table 1 along with standards for hcp Be [24] and the cubic $Be_{.67}B_{.33}$ phase. The crystallized phase closely matches the diffraction file for $Be_{.67}B_{.33}$ with one additional spacing that may be attributed to the (10.1) plane of the hcp Be phase. For this equiaxed and isotropic cubic structure, the grain size is 100 ± 4 nm as measured using the lineal intercept method.

The crystallization process in the $Be_{.975-n}B_nFe_{.018}Cr_{.004}Co_{.003}$ samples appears to be more sluggish than in the $Be_{.823}B_{.151}Cu_{.025}$ case. The as-deposited structure for n = .056 is amorphous as shown in the bright field image (of Fig. 2a) and does not change with heating to as high as 723 K. However, at 748 K, some granular contrast begins to appear in the bright field image of the $Be_{.919}B_{.056}Fe_{.018}Cr_{.004}Co_{.003}$ sample as indicated by the arrows (seen in Fig 2b). These regions are <20 nm in size. The SAD pattern at 748 K (as in the as-deposited condition) does not show any resolvable crystalline reflections, except the diffuse halo of the amorphous matrix appears. An average spacing of 0.165 ± 0.002 nm corresponds with the SAD pattern halos of the amorphous Be-B-X phases (shown in both Figs. 1a and 2a). A similar result is found for the n = .137 sample, where the onset of this diffraction contrast occurs at an even higher temperature of 773 K. Samples with greater concentrations of B did not show any changes from the as-deposited amorphous condition. Above 748 K, the cross-sectioned samples became unstable and disintegrated which prevents examination at higher temperatures. No changes were observed for the $Be_{.991-n}B_nFe_{.006}Cr_{.001}Co_{.001}$ (where .133<n) coatings during the in-situ anneal treatments.

The hardness results for the sputter deposited $Be_{.975-n}B_nFe_{.018}Cr_{.004}Co_{.003}$ coatings are plotted in Fig. 3. A continuous increase in the hardness is measured for these amorphous as-deposited coatings as the B concentration increases. Also, for comparison, previous results for the $Be_{1-x}B_x$ coatings are plotted in Fig. 3. [16] For the binary Be-B alloy deposits, the hardness value initially increases with increasing B content (n). These binary Be-B coatings are crystalline. The hardness of the Be-B coatings then decreases above 7 at.% B as the microstructure of the coating matrix changes from crystalline to amorphous.[16] The binary Be-B coatings are fully amorphous above the eutectic composition of 11 at.% B where the hardness then continues to increases with additional B content. Therefore, it appears that the crystalline Be-B coatings are harder than the counterpart $Be_{.975-n}B_nFe_{.018}Cr_{.004}Co_{.003}$ amorphous coatings for identical B concentrations (n) less than 10 at.%. The binary Be-B coatings would then appear to be softer than the Be-B-X coatings for n values above 10 at.% B. For reference, a nanoindentation value of 28 GPa is measured for the hardness of pure sputter deposited B coatings. [25]

ANALYSIS

The result of an as-deposited amorphous phase for $Be_{.823}B_{.151}Cu_{.025}$ (Fig. 1) is consistent with prior findings for the $Be_{1-x}B_x$ coatings produced by magnetron sputter deposition. [16, 18] In the binary Be-B system, an amorphous phase was found for compositions above the 11 at.% eutectic B concentration. [16] Diffusion-controlled crystallization for a 16 at.% B coating occurred at 473 K as crystallites >5 nm in size appeared to emerge within an amorphous matrix. [18] The temperature dependent evolution of nucleation sites for crystallization and the increasing

size of the nanocrystals in the 16 at.% B sample suggested a diffusion regulated process as did the appearance of phase separation in the SAD patterns. [18] In comparison to the $Be_{.84}B_{.16}$ case, the addition of 2.5 at.% Cu has further stabilized the amorphous ternary phase by increasing the crystallization temperature to 673 K. The close match of the $Be_{.823}B_{.151}Cu_{.025}$ interplanar spacings suggests crystallization as a variant of a cubic $Be_{.67}B_{.33}$ phase noting that the solubility of Cu is up to 10 at.% in Be. [13] However, the spontaneous appearance of crystallization as the temperature was increased to 673 K seems to suggest polymorphous crystallization, unlike the slower nucleation and growth process observed for $Be_{1-x}B_x$. [18] It would then appear that phase separation may not be as dominant during crystallization from the supersaturated $Be_{.823}B_{.151}Cu_{.025}$ amorphous phase.

The pseudo-ternary $Be_{1-m-n}B_nX_m$ coatings where $X = Fe_{.71}Cr_{.16}Co_{.13}$ are stable to even a higher temperature. As for the $Be_{1-x}B_x$ coatings, diffraction contrast within the amorphous matrix appears to continuously evolve with increasing temperature. For the pseudo-ternary, the onset temperature is at least 748 K (versus just 473 K for the $Be_{1-x}B_x$ binary system) even though definitive evidence of crystallization through SAD patterns has yet to be made for the $Be_{1-m-n}B_nX_m$ samples (where $X = Fe_{.71}Cr_{.16}Co_{.13}$) annealed to 773 K. As for the crystallization mechanism, the possibilities of glassy phase separation and primary plus secondary crystallization can't be excluded since detailed calorimetry at intermediate temperatures for these deposits on silicon is still lacking. A eutectic crystallization mechanism (or a variant thereof) may occur in which the glass transforms to the two crystalline phases growing in closely coupled form. After all, the average spacing associated with the amorphous halo for the Be-B-X phases is equivalent to the (220) $Be_{.67}B_{.33}$ spacing. In addition, the present result for the sputter deposited $Be_{.919}B_{.056}Fe_{.018}Cr_{.004}Co_{.003}$ sample reveals perhaps the most Be-rich (at 92 at.%) amorphous phase reported in the literature.

Synthesis of smooth robust coatings of $Be_{1-x}B_x$ that are a hundred microns thick for use as ignition capsules [8] will require a careful control of the residual stress state. A method to minimize residual stress is to control the working gas pressure during the sputter deposition. For example, the zero stress cross-over from compression to tension for dc sputtered Be and Be-B was shown to occur at 2.0 Pa and 2.7 Pa, respectively. [26] (For the Be-B target sputtered in the radio frequency mode, a tensile stress results at low working gas pressure and is minimized above 4 Pa. [26]) Therefore, a coating with less B would appear to be more favorable from a point of view on residual stress control – a criteria that supports the use of pseudo-ternary Be-B-X for capsule applications.

The addition of B to Be is expected to enhance the hardness of Be-B-X coatings because of contributions from grain boundary and solid solution strengthening (seen in the results plotted in Fig. 3) as well as the presence of defects, e.g. vacancies. [16] Previously, it was shown that neither grain boundary nor solid solution strengthening effects alone were sufficient to account for the increase in the hardness of the $Be_{1-x}B_x$ coatings. [16] Because of both strengthening effects, it seems that the hardness of $Be_{1-x}B_x$ coatings should increase monotonically with B concentration. However, the hardness value peaks at a concentration of about 7 at.% B. A further increase in B concentration, in fact, causes a decrease in hardness. This decrease in hardness with increasing B concentration coincides with the onset presence of the amorphous phase. [16] Mechanically, an amorphous structure can be expected to be softer than its crystalline counterparts. For example, it has been shown that amorphous alumina is softer than its crystalline counterparts. [27] Also, it has been reported that an amorphous alloy containing nanocrystals is harder than the amorphous structure alone. [28-29] For the two-phase microstructures that are a mixture of crystalline and amorphous, the mechanism of deformation may be similar to that proposed in an Al-base amorphous alloy containing fcc-Al nanocrystals.

[30] Deformation of the two-phase mixture occurs in the soft amorphous matrix where the nanocrystals can be treated as hard dispersoids. For the fully amorphous $Be_{.975-n}B_nFe_{.018}Cr_{.004}Co_{.003}$ coatings, the continuous increase in hardness with increased B concentration is simply caused by the intrinsically hard B. The 28 GPa hardness of pure B is much greater than the 9.5 GPa hardness for sputter-deposited pure Be.

In general, the lower temperatures observed for the crystallization of the sputter deposited $Be_{1-x}B_x$ coatings with respect to the melting point would seem to indicate that the stabilization of a Be-rich amorphous phase in the bulk may be difficult. [18] The sputter deposition process does produce very fast quench rates from the vapor to the solid phase that can easily be several orders of magnitude greater than for processes even as melt spinning. However, for the pseudo-ternary Be-B-X alloys as the amorphous $Be_{.975-n}B_nFe_{.018}Cr_{.004}Co_{.003}$ phase, the reduced glass transition temperature (which is less than the crystallization temperature) [31-32] may be approaching $0.51 \bullet T_m$ noting a crystallization temperature of >748 K and a corresponding melt point (T_m) of about 1475K. Thus, a potential bulk glass former may exist as ratios of about 0.50 to 0.66 or larger are often associated with bulk glass formation.

SUMMARY

Ternary and pseudo-ternary Be-B-X coatings are prepared through the method of sputter deposition. The coating hardness is characterized using nanoindentation testing. The coating structure is assessed, using transmission electron microscopy, in both the as-deposited condition and as subjected to in-situ thermal anneal treatments. The addition of small concentrations of the ternary element (X), e.g. at the equivalence of 2.5 at.% and less, produces an amorphous Be-B-X

structure in the as-deposited condition. Frustration of the path to crystallization is evidenced as the kinetics and mode of crystallization process slow as X = Fe-Cr-Co is used in place of X = Cu. The onset of crystallization increases as well from 673 K for X = Cu to temperatures greater than 748 K for X = $Fe_{.71}Cr_{.16}Co_{.13}$. In comparison, amorphous Be-B binary alloy coatings were found to start crystallizing at temperatures as low as 473 K. The hardness of the as-deposited amorphous Be-B-X coatings (for X = $Fe_{.71}Cr_{.16}Co_{.13}$) varies continuously and increases with the B concentration suggesting a form of solid solution strengthening. The ternary alloy of $Be_{.919}B_{.056}Fe_{.018}Cr_{.004}Co_{.003}$ provides an example of the reduced B concentration needed to stabilize an amorphous deposit that is softer as well, in comparison to the binary Be-B system where B concentrations greater than the 11 at.% B eutectic are required for an amorphous structure. The improved thermal stability and reduced hardness of the Be-B-X coating suggest a useful material alternative for the fabrication of ignition capsules in application for inertial confinement fusion.

ACKNOWLEDGMENTS

The authors thank Phil Ramsey and Mark McKernan for their contributions to the synthesis of the coatings, and to Bill Choi for his contributions to the hardness measurements. This work was performed under the auspices of the U.S. Department of Energy by University of California, Lawrence Livermore National Laboratory under contract No. W-7405-Eng-48.

REFERENCES

1. D. Webster and G.J. London, Beryllium Science and Technology Vol. **1**, (Plenum Press, New York and London, 1979).

2. D.R. Floyd and J.N. Lowe, Beryllium Science and Technology Vol. **2**, (Plenum Press, New York and London, 1979).

3. R.J. Switz, in Beryllium Science and Technology Vol. **2**, pp. 231-247, edited by D.R. Floyd and J.N. Lowe (Plenum Press, New York and London, 1979).

4. L.A. Grant, in Beryllium Science and Technology Vol. **2**, pp. 249-273, edited by D.R. Floyd and J.N. Lowe (Plenum Press, New York and London, 1979).

5. T.G. Nieh and J. Wadsworth, Scripta Mater. **38**, p. 863 (1998).

6. A. Aldinger and G. Petzow, in Beryllium Science and Technology Vol. **1**, pp. 235-305, edited by D. Webster and G.J. London (Plenum Press, New York and London, 1979).

7. T.G. Nieh and J. Wadsworth, Scripta Metall. Mater. **24,** p. 1489 (1990).

8. S. Haan, Phys. Plasmas **2**, p. 2480 (1995).

9. C.W. Chen and C.S. Alford, J. Vac. Sci. Technol. **A6**, p. 128 (1988).

10. R. M^{c}Eachern, C. Alford, R. Cook, D. Makowiecki, and R. Wallace, Fusion Technol. **31**, p. 435 (1997).

11. A.F. Jankowski, P. Ramsey, M. M^{c}Kernan, and J.D. Morse, in Amorphous and Nanostructured Carbon Vol. **593**, pp. 489-592, eds. J. Robertson, J. Sullivan, O. Zhou, T. Allen, and B. Coll (Mater. Res. Soc. Symp. Proc., Pittsburgh, PA, 2000).

12. A. Jankowski, in Structure and Mechanical Properties of Nanophase Materials Vol. **634**, Ch. 3, pp 15.1-6, ed. D. Farkas, H. Kung, M. Mayo, H. van Swygenhoven, and J. Weertman (Mater. Res. Soc. Symp. Proc.**,** Pittsburgh, PA, 2001).

13. T. Massalski, (ed.), in Binary Alloy Phase Diagrams, pp. 341-2 (ASM International, Metals Park, OH, 1987).

14. J.W. Donald and H.A. Davies, J. Non-Cryst. Sol. 30 (1978) 30.

15. J.B. Holt, D.C. Akeny and C.F. Cline, Scripta Metal. 14 (1980) 959.

16. A.F. Jankowski, M.A. Wall, A.W. Van Buuren, T.G. Nieh, and J. Wadsworth, Acta Mater. 50 (2002) 4791.

17. H. Liebermann, in Amorphous Metallic Alloys, pp.26-41, ed. F. Luborsky (Butterworth and Co. Publ., London, G.B., 1983).

18. A.F. Jankowski, M.A. Wall, and T.G. Nieh, J. Non-Cryst. Sol. 317 (2003) 129.

19. W.L. Johnson, Mater. Res. Soc. Bull. 24(10) (1999) 42.

20. A. Peker and W.L. Johnson, Appl. Phys. Lett. 63 (1993) 2342.

21. X.H. Lin and W.L. Johnson, J. Appl. Phys. 78 (1995) 6514.

22. S.B. Newcomb, C. Boothroyd, and W. Stobbs, J. Microsc. **140**, p. 195 (1985).

23. M. Doerner and W.D. Nix, J. Mater. Res. **1**, p. 601 (1986).

24. J. M^{c}Kay and M. Hill, J. Nucl. Mater. **8**, p. 263 (1963).

25. A. Jankowski, J. Hayes, M. M^{c}Kernan and D. Makowiecki, Thin Solid Films **308-9**, p. 94 (1997).

26. E. Hsieh, C. Gillespie, E. Pierce, and C. Hatcher, J. Vac. Sci. Technol. A **6**, p. 1893 (1988).

27. T.C. Chou, T.G. Nieh, S.D. M^{c}Adams, and G.M. Pharr, Scripta Metall. Mater. **25**, p. 2203 (1991).

28. H. Chen, Y. He, G.J. Shiflet, and S.J. Poon, Scripta Metall. Mater. **25**, p. 1421 (1991).

29. A. Inoue, H.M. Kimura, K. Sasamori, and T. Masumoto, Mater. Trans. JIM **35**, p. 85 (1994).

30. Y.-H. Kim, A. Inoue, and T. Masumoto, Mater. Trans. JIM **31**, p. 747 (1990).

31. D. Turnbull, J.C. Fisher, J. Chem. Phys. 17 (1949) 71.

32. D. Turnbull, J. Chem. Phys. 18 (1950) 198.

TABLE I. Interplanar spacings (nm) of crystallized BeBCu alloy

hexagonal Be		cubic $Be_{.67}B_{.33}$		$Be_{.823}B_{.151}Cu_{.025}$
(hk.l)	d(nm)	(hkl)	d(nm)	d(nm) at 673 K
-	-	(111)	0.2690	0.267
-	-	(200)	0.2335	0.230
(10.0)	0.1980	-	-	-
(00.2)	0.1793	-	-	-
(10.1)	0.1733	-	-	0.174
-	-	(220)	0.1648	0.162
-	-	(311)	0.1407	0.141
(10.2)	0.1329	(222)	0.1347	0.132

FIGURE CAPTIONS

Figure 1. – High resolution and bright field transmission electron microscope images are shown, respectively, as viewed in cross-section along with selected-area diffraction patterns (inserts) for sputter-deposited $Be_{.823}B_{.151}X_{.025}$ coatings where X is Cu in (a) the as-deposited condition, and (b) as crystallized at an anneal temperature of 673 K.

Figure 2. – Bright field transmission electron microscope images are shown as viewed in cross-section along with selected-area diffraction patterns (inserts) for sputter-deposited $Be_{.917}B_{.056}X_{.025}$ coatings where X is $Fe_{.71}Cr_{.16}Co_{.13}$ in (a) the as-deposited condition, and (b) at an anneal temperature of 748 K.

Figure 3. – The variation of Hardness (GPa) with B concentration is shown for sputter deposited coatings of $Be_{1-m-n}B_nX_m$ for m = 0 and 0.025 where X is $Fe_{.71}Cr_{.16}Co_{.13}$.

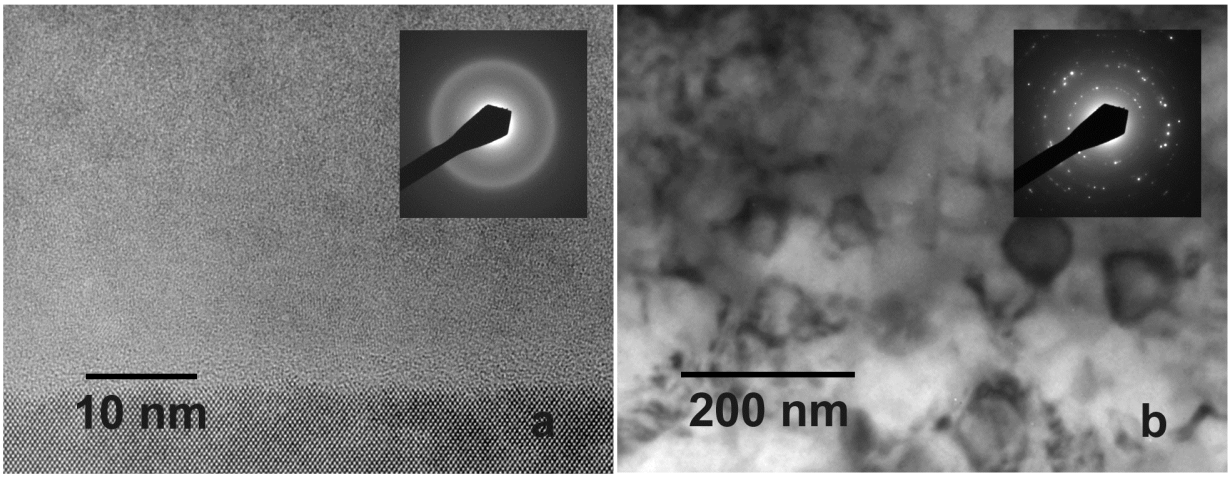

Figure 1.

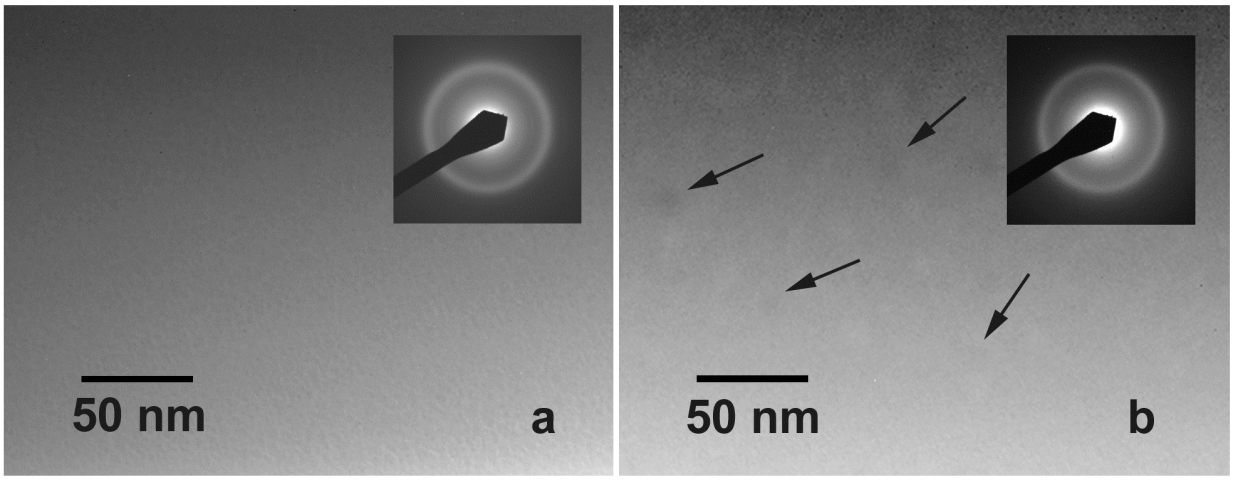

Figure 2.

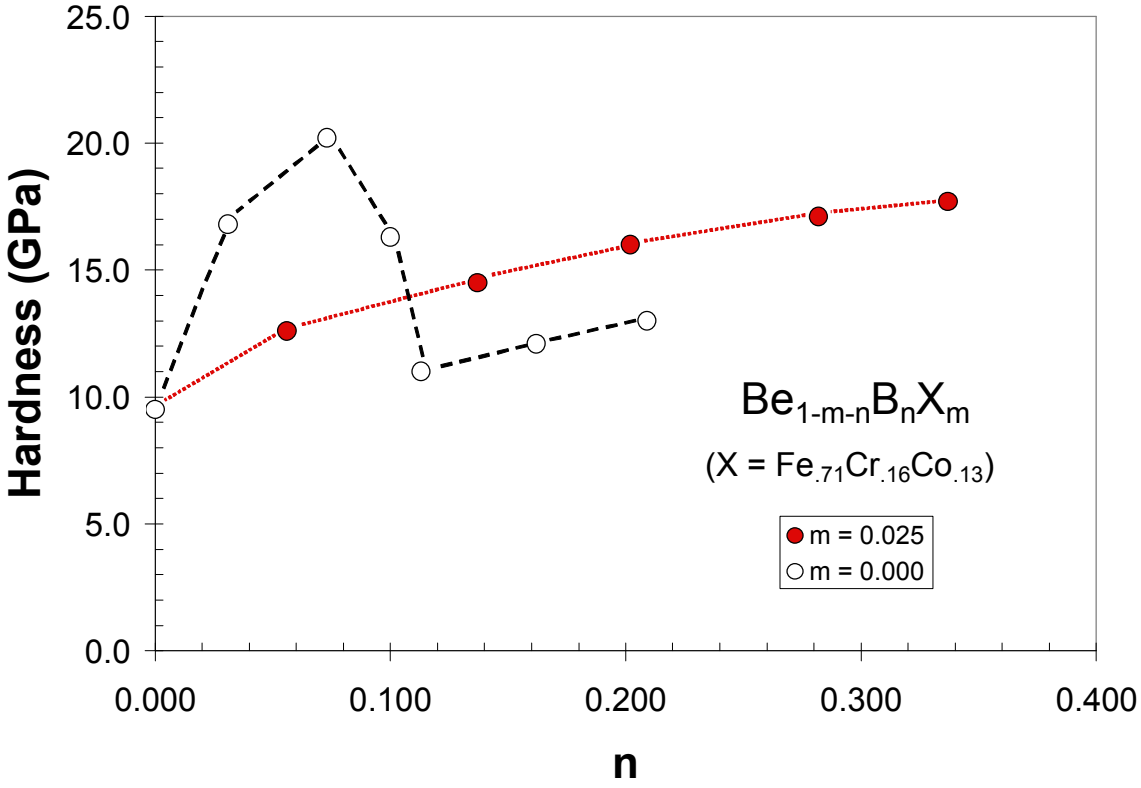
25.0
20.0
15.0
10.0
5.0
0.0
Hardness (GPa)
0.000
0.100
0.200
0.300
0.400
n
Be1-m-nBnXm
(X = Fe.71Cr.16Co.13)
m = 0.025
m = 0.000

Figure 3.